



# Impacts of low-frequency climate variability on tropical cyclone activity in the North Indian Ocean basin

Kanak Lata Xalxo<sup>1</sup> · Biranchi Kumar Mahala<sup>1</sup> · Pratap Kumar Mohanty<sup>2</sup> · Ashish Routray<sup>3</sup> · Sarbeswar Mohanty<sup>4</sup>

Received: 21 February 2023 / Accepted: 27 August 2023 / Published online: 4 September 2023  
© The Author(s), under exclusive licence to Springer-Verlag GmbH Austria, part of Springer Nature 2023

## Abstract

The impact of the Indian Ocean Dipole (IOD) and El Niño Southern Oscillation (ENSO) on tropical cyclone activities in the North Indian Ocean (NIO) basin including the Bay of Bengal (BoB) and Arabian Sea (AS) are investigated using data from 1891 to 2020 of the cyclone e-Atlas developed by India Meteorological Department, Niño 3.4, and the Indian Ocean Dipole mode indices (DMI). A total of 657 tropical cyclones are observed over the NIO basin with an annual frequency of 5.05 while the annual frequencies over BoB and AS are 4.03 and 1.02, respectively. The years from 1891 to 2020 have been classified as years of ENSO [El Niño (EN), La Niña (LN), and neutral ENSO (nENSO)] and IOD [positive IOD (pIOD), negative IOD (nIOD), and noIOD] years. The frequency is higher in EN (nIOD) followed by LN (noIOD) years in the NIO basin. LN (EN) events and nIOD (pIOD) events favor tropical cyclone cases in the BoB (AS). Tropical cyclone genesis has a peak density covering 10–15° N in the BoB and AS during ENSO and IOD years. Wavelet coherence (WTC) analysis between the frequency of tropical cyclones over the NIO basin and the DMI/Niño 3.4 index shows high coherence with DMI and in-phase relationship for the period 2006–2020 while it shows higher coherence with Niño 3.4 index and out-of-phase relationship for the period 1991–2020. The WTC analysis is also performed separately for BoB and AS. Multiple linear regression analysis of the frequency of tropical cyclones and Niño 3.4 index/DMI shows a significant correlation between the frequency and the DMI. A strong coherence between DMI and Niño 3.4 index is also found for the period 1991–2001 over the NIO basin.

## 1 Introduction

Although the North Indian Ocean (NIO) is a less active basin in terms of tropical disturbances, the basin produces some of the deadliest cyclones in the globe. Since climate projections show that the Indian Ocean will continue to warm rapidly along with an increase in the intensity of

cyclones in this basin, changes in ocean-cyclone interactions that have recently emerged in response to this warming need to be closely monitored (Singh and Roxy 2022). In recent decades, sea surface temperatures (SSTs) contributing to cyclogenesis in the Arabian Sea (AS) have been 1.2–1.4 °C higher than SSTs four decades ago. Rapid warming in the NIO, caused by global warming, tends to increase heat flow from the ocean to the atmosphere and favors cyclone intensification. El Niño-Southern Oscillation (ENSO) and the Indian Ocean Dipole (IOD) are two prominent and significant low-frequency climate phenomena in the tropical ocean-atmosphere coupled system. ENSO and IOD have far-reaching consequences that extend far beyond the basins in which they form, the tropical Pacific and Indian Ocean, respectively.

ENSO is one of the most important climate variability phenomena in the world due to its ability to change the global climate affecting the global temperature and precipitation. A deeper thermocline and weaker-than-normal surface divergence, or convergence in the westerly wind results in the warm extreme, called El Niño, while

✉ Biranchi Kumar Mahala  
biranchimahala@gmail.com

<sup>1</sup> Department of Mathematics, School of Applied Sciences, Kalinga Institute of Industrial Technology (KIIT) Deemed to be University, Bhubaneswar, Odisha, India

<sup>2</sup> Department of Marine Sciences, Berhampur University, Berhampur, Odisha, India

<sup>3</sup> National Centre for Medium Range Weather Forecasting (NCMRWF), Ministry of Earth Sciences, Noida, Uttar Pradesh, India

<sup>4</sup> Department of Economics, School of Humanities, Kalinga Institute of Industrial Technology (KIIT) Deemed to be University, Bhubaneswar, Odisha, India

a shallow thermocline and stronger-than-normal surface divergence results in the cold extrema, called La Niña (McPhaden 2004).

In the northwest Pacific, ENSO is considered to be the dominant factor controlling the interannual variability in tropical cyclone activity (Chan 2007). Many researchers have extensively studied the tropical cyclone activities in the northwest Pacific in relation to ENSO (Camargo et al. 2007b, 2007c, 2007a; Camargo and Sobel 2005; Chia and Ropelewski 2002; Wang and Chan 2002; Webster et al. 2005; Wu et al. 2004). The frequency of typhoons is higher during warm ENSO periods over a majority of basins in the northwest Pacific (Saunders et al. 2000). China experiences the greatest number of landfalling tropical cyclones during the late season of La Niña (LN) years in the northwest Pacific (Wu et al. 2004). The study by Bhardwaj et al. (2019) shows that LN events characterize more frequent and intense tropical cyclones than EN events. Their study period was 1972–2015 and only for BoB post-monsoon season.

The IOD, is a mode of climate variability in the Indian Ocean that evolves in spring (May–June), peaks in fall (October–November), and terminates in early winter (December) (Murtugudde et al. 2000; Saji et al. 1999; Webster et al. 1999). Various past studies have investigated the influence of IOD on various sectors in East Africa and Indonesia (Saji et al. 1999), the Asian (Ashok et al. 2001), and Australian (Cai and Cowan 2008; Ummenhofer et al. 2009) summer monsoon regions. A positive IOD (pIOD) is characterized by cooler than normal water in the eastern tropical Indian Ocean and warmer than normal water in the western tropical Indian Ocean (Saji et al. 1999) while a reverse pattern characterizes a negative IOD (nIOD).

Classification of ENSO and IOD years has been studied by many researchers/scientists using various methods for different periods (Girishkumar and Ravichandran 2012; Grimm et al. 2000; Lestari and Koh 2016; Liu and Chan 2003; Mahala et al. 2015; Meyers et al. 2007; Power et al. 2021; Yuan and Li 2008). There is a reduction in tropical cyclone activity over BoB during severe cyclone months of May and November during the warm phase of ENSO (Singh et al. 2000). The study by Singh et al. (2001) shows that the frequency of formation of monsoon depressions in the BoB increases during warm ENSO phases. ENSO and IOD have impacted the Indian summer monsoon on local and regional scales between 2015 and 2016. The study by Sreelekha and Babu (2019) suggests that nIOD may cause large scale variation in circulation patterns resulting a deficit in Indian summer monsoon rainfall. The intensity and phenomena of the Indian Ocean Dipole are measured by the dipole mode index (DMI) (Saji et al. 1999). Both IOD and El Niño (EN) can be classified according to the zonal distribution of the SST anomalies (SSTA) in the eastern and central Pacific (Ashok et al. 2007; Capotondi et al.

2015; Chen et al. 2015; Kao and Yu 2009) or by the time of onset (Xu and Chan 2001).

The study by Yuan and Cao (2013) shows that during negative IOD (nIOD) events, SSTA is positive east of 90° E in the tropical southeast Indian Ocean and negative in the west of 80° E in the tropical western Indian Ocean as a result, the low-level cyclonic circulations are more significant, which strengthen the convection over the BoB and eastern AS, and generate a positive vorticity anomaly at low-level. These factors are favorable for the increasing tropical cyclone genesis in the NIO. Zhou et al. (2019) studied the impact of IOD on the interannual variability of tropical cyclone activity in the northwest Pacific from 1961 to 2015. Their study suggests that the number of tropical cyclones making landfall in China is negatively correlated with DMI. Roose et al. (2022) have studied the interannual variability of low-latitude post-monsoon cyclones formed in the BoB for the period 1979–2020 and their teleconnection with ENSO and IOD. The study indicates that relative vorticity is a vital parameter influencing the interannual variability of low-latitude BoB cyclones.

The climate drivers ENSO and IOD are linked by the Walker circulation connecting the Pacific and Indian Oceans, such as EN-pIOD and LN-nIOD (McKenna et al. 2020). The study by Ashok et al. (2003) suggests that the IOD is a unique and independent climate mode in the Indian Ocean. Previous studies (Du et al. 2013; Fan et al. 2017; Hong et al. 2008) show that an atmospheric bridge connecting ENSO with the Indian Ocean can trigger an IOD event and modulate its evolution. In addition, the studies by Du et al. (2013) and Sun et al. (2015) show that IOD is a combination of internally forced and ENSO-driven phenomena. However, the onset, peak, and decay of an IOD can vary to some extent due to ENSO (Capotondi et al. 2015; Santoso et al. 2012). Yuan and Cao (2013) used wavelet coherence (WTC) analysis between the NIO tropical cyclone frequency and DMI for the period 1981–2010. Their study showed a statistically significant relationship between the frequency of NIO tropical cyclones and IOD events. Wavelet analysis is increasingly becoming an efficient tool for the trend analysis of various time series (Grinsted et al. 2004; Ng and Chan 2012). Ng and Chan (2012) used wavelet analysis to investigate the impact of ENSO-IOD on tropical cyclone activity in the northwest Pacific. Their study suggests that the combination of DMI and ENSO Modoki index gives worse results for the northwest Pacific. However, the possible linkages between the ONI (or Niño 3.4)/the DMI, and the tropical cyclone frequency in the NIO basin are not reported so far.

Our goal is to understand and improve knowledge about the impact of climate variability on tropical cyclone activity in the NIO basin using climatology and digital tools. In the present study, the ENSO and IOD years are classified from 1891 to 2020. Frequency, decadal variability, and genesis

locations of tropical cyclones in the NIO basin, BoB, and AS under different ENSO and IOD events are discussed. An investigation using wavelet analysis of the ENSO-IOD-related impact on the tropical cyclone activity over the NIO basin is conducted. Section 2 explains the data source, the basis for the classification of ENSO and IOD years, the wavelet coherence method, and the multiple linear regression method. The results and discussion are presented in Section 3 and the conclusion in Section 4.

## 2 Data sources and methodology

### 2.1 Data sources

The present work is a study examining the impact of ENSO and IOD on tropical cyclone activities in the NIO basin. The main data source is the cyclone e-Atlas (version 2.0/2011) developed by India Meteorological Department (RSMC 2011) which is an electronic version based on updated and digitized data for the period 1891–2022. The data from 1891 to 2020 are collected from the cyclone e-Atlas-IMD (<https://14.139.191.203/AboutEAtlas.aspx>). The e-Atlas provides detailed information on cyclonic disturbances such as depression, cyclonic storms (CS), and severe cyclonic storms or more (SCS). The classification of depression, CS, and SCS has been made as per RSMC (2011). One of the various ENSO indicators that are based on the SSTA is the Niño 3.4 index ([https://psl.noaa.gov/gcos\\_wgsp/Timeseries/Data/nino34.long.anom.data](https://psl.noaa.gov/gcos_wgsp/Timeseries/Data/nino34.long.anom.data)). EN and LN events are usually defined by the Niño 3.4 and the Oceanic Niño indices (Mahala et al. 2015; Trenberth and Stepaniak 2001). DMI is used to classify the years 1891–2020 as pIOD, nIOD, and noIOD years. DMI data were extracted from National Oceanic and Atmospheric Administration (NOAA) Physical Science Laboratory ([https://psl.noaa.gov/gcos\\_wgsp/Timeseries/Data/dmi.had.long.data](https://psl.noaa.gov/gcos_wgsp/Timeseries/Data/dmi.had.long.data)) for the analysis.

### 2.2 A basis for classification of the ENSO and IOD years

Various methods and indicators have been applied previously to classify the ENSO events viz., SST-based indices (Niño 1+2, Niño 3, Niño 4, Niño 3.4, Oceanic Niño Index (ONI), Trans-Niño Index), and surface atmospheric pressure indices (Southern Oscillation Index and Multivariate ENSO Index) (Islam 2018). The Niño 3.4 index and the ONI are the most powerful indices used to categorize EN and LN events. The details on the statistical classification of ENSO years are available in the studies by Singh et al. (2011) and Meyers et al. (2007). The strength of EN and LN events is monitored by Niño 3.4 index. Niño 3.4 index is the average SSTA for the region from latitude 5° S to 5° N and longitude

120°–170° W. This region exhibits colossal variability on the EN timescale and is close to regions where local SST changes are important to shift large areas of precipitation mostly found in the far western Pacific. A year is categorized as EN (LN) when the 5-month running mean of the Niño 3.4 index goes beyond +0.4 (−0.4) °C for at least 6 months in succession (<https://climatedataguide.ucar.edu/climate-data/nino-sst-indices-nino-12-3-34-4-oni-and-tni>).

Niño 3.4 index is used to classify the years from 1891 to 2020 as EN, LN, and neutral ENSO

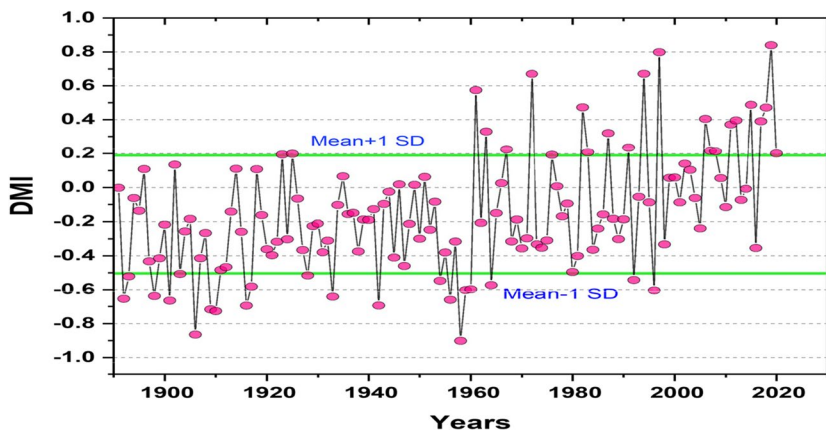
(nENSO). Oceanic Niño Index (ONI) data have been used ([https://origin.cpc.ncep.noaa.gov/products/analysis\\_monitoring/ensostuff/ONI\\_v5.php](https://origin.cpc.ncep.noaa.gov/products/analysis_monitoring/ensostuff/ONI_v5.php)) only to compare for classification made in the study by Mahala et al. (2015).

There is an anomalous SST gradient or DMI between the tropical western Indian Ocean (50°–70° E, 10° S–10° N) and tropical southeastern Indian Ocean (90°–110° E, 10° S–0°). DMI is used to identify the intensity of the IOD. When the DMI is positive (negative), the phenomena are referred to as pIOD (nIOD). We used the DMI to classify the year from 1891 to 2020 as pIOD, nIOD, and noIOD years. Each year, the DMI's arithmetic mean for the 6 months from June to November is determined, and the estimated value is assigned to that year as a DMI representative (Mahala et al. 2015). Furthermore, we have computed the mean and the standard deviation (SD) of the DMI for the study period (1891–2020). The year is classified as pIOD (nIOD) when the mean DMI is greater (less) than or equal to the mean +1 SD (−1 SD) (Fig. 1).

### 2.3 Wavelet coherence method

Predictable behavior in geographical time series such as periodicity and trend are of great interest. Most mathematical models examine periodicities in the frequency domain. However, wavelet transforms expand the time series into time-frequency space and find localized intermittent periodicities (Grinsted et al. 2004). The concept of wavelet is applied in various fields where data on time series has a crucial role. Wavelet analysis is a common technique for analyzing localized fluctuations in a time series. The wavelet transform is a generalized form of the Fourier transform (FT) and windowed FT (WFT) (Gabor 1946). Many past studies explained the wavelet transform with examples (Aguilar-Conraria and Soares 2014; Lau and Weng 1995; Maraun and Kurths 2004; Torrence and Compo 1998). Wavelet transform uses generalized local basis functions (wavelets) that can be stretched and translated with frequency and time. A flexible window can be adapted to the entire time-frequency domain considered the wavelet domain (WD). WD narrows (widens) when focusing on high-frequency (low-frequency) signal backgrounds. Due to the “uncertainty principle” (Chui 1992), the height and the width of the

**Fig. 1** Classification of IOD years based on DMI data and its standard deviation (SD)



time-frequency window cannot be arbitrary. The following discussion is based on the Morlet wavelet, and the mother wavelet is defined as,

$$\Psi(t) = \pi^{-1/4} e^{i\omega_0 t}$$

with  $\omega_0$  as the non-dimensional frequency, and  $t$  denotes time. Mathematically, the family of the Morlet wavelet  $\omega_{a,b}(t)$  can be generated by the time translation and scale dilations such that

$$\omega_{a,b} = \frac{1}{a^{1/2}} \Psi\left(\frac{t-b}{a}\right)$$

where  $a (> 0)$  denotes the scale (dilation) and  $b$  denotes the position (translation) of the wavelet;  $\omega_{a,b}(t)$  is called “daughter wavelet” or “wavelet”.

In a time-series consisting of  $N$  number of points, the convolution of the wavelet with the series value is computed by the formula,

$$W_n(s) = \sum_{n'=0}^{N-1} z_{n'} \Psi^* \left[ \frac{(n' - n) \delta t}{s} \right]$$

where,  $n'$  = index of time series  $z$ ,  $n$  = localized time index of normalized wavelet  $\Psi$ ,  $\Psi^*$  = complex conjugate of the mother wavelet,  $s$ , and  $t$ , respectively, denote scale and time.

The cross-wavelet transform of two-time series,  $a(t)$  and  $b(t)$  was developed by Hudgins et al. (1993). The two-time series A and B are compared through the “cross-wavelet spectrum.” If  $W_n^A(s)$  and  $W_n^B(s)$  are the wavelet transforms of the series A and B, then the cross-wavelet spectrum is given by:

$$W_n^{AB}(s) = W_n^A(s) \cdot W_n^{B*}(s)$$

with a power  $|W_n^{AB}(s)|$ . Wavelet coherence is used to analyze the cross-wavelet transform’s degree of coherence over time-frequency space (Chang et al. 2019; Torrence and Webster 1998). It helps to determine the dominant modes of

variability and their variation with time besides quantifying the relationship between climate forcings and the frequency of tropical cyclones. Furthermore, it also shows whether the parameters are correlated and if so, are they in-phase or out-of-phase. A detailed study on WTC computation is available in past studies by Grinsted et al. (2004) and Schulte et al. (2016). In the present study, wavelet coherence is calculated using the “biwavelet” package in “R-programming” software.

### 2.4 Multiple linear regression

The objective of the current study is to find the plausible linkage between tropical cyclone frequency and climate modes, such as ENSO and IOD. Multiple linear regression is a method (Mostafa 2020) for analyzing the connection between one dependent variable and more than one independent variable (climatic indices). The multiple linear regression is given by,

$$y_i = \alpha_0 + \alpha_1 x_{i1} + \alpha_2 x_{i2} \dots \dots \dots + \alpha_p x_{ip} + \epsilon_i; i = 1, 2, \dots \dots N$$

where,  $y_i$  a dependent variable,  $x_{ip}$  an independent variable,  $\alpha_0$  as intercept,  $\alpha_1, \alpha_2, \dots, \alpha_p$  the  $x$ ’s coefficient and  $\epsilon_i$  is a residual term that the model always keeps it contributing as minimum as possible.

## 3 Results and discussion

### 3.1 Events of ENSO and IOD

In the impact analysis of ENSO and IOD, Niño 3.4 data for the period from 1891 to 2020 are used to classify the years into EN, LN, and nENSO events. DMI data is also used to classify the years of pIOD, nIOD, and noIOD. The classification of years into EN, LN, nENSO, pIOD, noIOD, and nIOD as well as their co-occurrence for the period

1891–2020 are presented in Table 1. Different investigators have used different methods for the classification of ENSO and IOD years for different periods (Girishkumar and Ravichandran 2012; Mahala et al. 2015; Meyers et al. 2007; Yuan and Li 2008). In the period 1891–2020, 38 years are categorized as EN years, 42 LN years, and 50 nENSO years while 23 as pIOD, 21 as nIOD, and 86 as noIOD years. The classification of ENSO-IOD years for the period in the present study matches exactly with the classification made by Girishkumar and Ravichandran (2012), although they made the analysis for a comparatively smaller period of 18 years (1993–2010) only and Mahala et al. (2015) in which they considered the period 1891–2007.

### 3.2 Frequency of tropical cyclones

Table 2 shows the statistics of the frequency of tropical cyclones in the NIO basin, BoB, and AS under different ENSO-IOD conditions. In 130 years of the study period from 1891 to 2020, a total of 657 tropical cyclones have occurred in the BoB and AS at 5.05 tropical cyclones per year whereas the study by Mahala et al. (2015) shows 502 tropical cyclones for the period 1891–2007 over BoB, and Mohanty et al. (2012) as 606 cyclonic disturbances (deep depressions, CS, and SCS or more intensity) over BoB for the period 1891 to 2010. In the NIO basin, a total of 195, 247, and 215 tropical cyclones are noted respectively in EN, nENSO, and LN years, while it is 107, 120, and 430 in pIOD, nIOD, and noIOD years. The average frequency of tropical cyclones during EN, nENSO, and LN years is computed as 5.13, 4.94, and 5.11, respectively, while it is 4.65, 5.0, and 5.71 during pIOD, noIOD, and nIOD years. Moreover, the frequency of tropical cyclones is computed as 5.28 for EN with pIOD and 6.15 for LN with nIOD. From the analysis, it is observed that the tropical cyclone frequency in the NIO basin is higher during EN (nIOD) years followed by LN (noIOD) years.

During the period 1891–2020, the frequency of tropical cyclones in the BoB is 4.17 (3.89) in LN (EN) years

**Table 2** Frequency of tropical cyclones over the NIO basin, BoB, and AS in different ENSO and IOD events.

	NIO basin	BoB	AS
1891–2020	657 (5.05)	524 (4.03)	133 (1.02)
EN	195 (5.13↑)	148 (3.89↓)	047 (1.24↑)
LN	215 (5.11↑)	175 (4.17↑)	040 (0.95↓)
nENSO	247 (4.94↓)	201 (4.02↓)	046 (0.92↓)
pIOD	107 (4.65↓)	078 (3.39↓)	029 (1.26↑)
nIOD	120 (5.71↑)	096 (4.57↑)	024 (1.14↑)
noIOD	430 (5.00↓)	350 (4.07↑)	080 (0.93↓)

The figures inside the bracket represent the frequency. The up/down arrows denote the increase/decrease in frequency from the climatological mean

while it is 0.95 (1.24) in the AS. In nIOD (pIOD) years, the frequency of tropical cyclones is 4.57 (3.39) over the BoB, while it is 1.14 (1.26) in the AS. During the EN, LN, and nIOD years, the frequency of tropical cyclones in the NIO basin is more than the climatological mean, while it is less in nENSO, pIOD, and noIOD years. During LN, nIOD, and noIOD years, the frequency of tropical cyclones in the BoB is more than the climatological mean, while it is less in EN, nENSO, and pIOD years. In the AS, the frequency of tropical cyclones is more than the climatological mean during EN, pIOD, and nIOD years, while it is less in LN, nENSO, and noIOD years. The analysis indicates that LN (EN) events of ENSO and nIOD (pIOD) events of the IOD favor the tropical cyclone cases in the BoB (AS). The results corroborate the study by Mahala et al. (2015). However, the frequency of BoB tropical cyclones during the period 1951–2020 is 3.48 (3.25) in LN (EN) years while it is 1.13 (1.42) for the AS. Previous studies (Girishkumar and Ravichandran 2012; Mahala et al. 2015) show the frequency of tropical cyclones in the BoB is more in LN years. However, the study period was for the BoB post-monsoon season of 1993–2010 by Girishkumar and Ravichandran (2012) and the entire calendar year in the BoB for the period 1891–2007 by Mahala et al. (2015).

**Table 1** Years of ENSO and IOD events from 1891 to 2020 (the numbers within the bracket indicate the total number of years)

	EN (38)	nENSO (50)	LN (42)
nIOD (21)		1901 1917 1928 1958 1959 1960 1992 1996	1892 1893 1898 1903 1906 1909 1910 1916 1933 1942 1954 1956 1964
noIOD (86)	1896 1899 1900 1902 1904 1905 1914 1918 1919 1930 1940 1941 1951 1957 1965 1968 1969 1977 1986 1993 2002 2004 2009 2014	1891 1895 1897 1907 1911 1912 1913 1915 1920 1921 1926 1927 1929 1931 1932 1935 1936 1937 1939 1943 1944 1946 1947 1948 1952 1953 1962 1966 1978 1979 1980 1981 1990 2001 2003 2005 2013 2016	1894 1908 1922 1924 1934 1938 1945 1949 1950 1955 1970 1971 1973 1974 1975 1984 1985 1988 1989 1995 1998 1999 2000 2010
pIOD (23)	1923 1925 1963 1972 1976 1982 1987 1991 1994 1997 2006 2015 2018 2019	1961 1967 2008 2012	1983 2007 2011 2017 2020

A proper analysis of the climatology of tropical cyclones including CS and SCS is indicative of the rapid intensification of tropical cyclones (Kranthi et al. 2023). An investigation has been made on the impact of ENSO and IOD on tropical cyclones with different intensities over the BoB, AS, and NIO basins for the period 1891–2020 (Table 3). Considering the intensity of tropical cyclones with intensity as SCS or more, it is observed that the maximum frequency in the BoB is 1.98 (2.22) during LN (pIOD) years, while it is 2.36 (2.81) for nENSO (nIOD) years for the CS. In the AS, the frequency of SCS is 0.87 (0.91) during EN (pIOD) years. In the NIO basin, the frequency of SCS is 2.71 (3.13) during EN (pIOD) years, while it is 2.8 (3.24) during nENSO (nIOD) years for the CS. A close inspection of the data shows that BoB experiences maximum frequency of SCS during LN years. In the AS and NIO basin, the frequency of SCS (CS) is more in EN (LN) years. The frequency of SCS (CS) in the BoB and the NIO basin is more in pIOD (nIOD) years. Looking at the frequency of tropical cyclones with intensity SCS or more, it is clear that EN year shows the most severe cyclonic storms in the NIO basin. However, the study by Girishkumar and Ravichandran (2012) suggests

that the LN year shows more SCS during the post-monsoon season of 1993–2010. The maximum frequency of SCS in the NIO basin during EN years is due to more SCS cases observed in the AS.

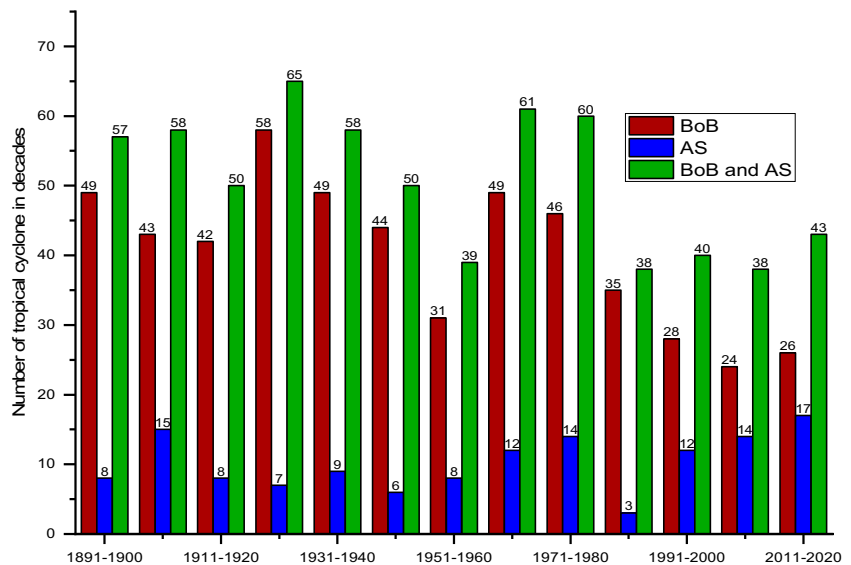
Furthermore, the total number of tropical cyclones in the decades through 1891–2020 is computed to investigate the decadal variability (Fig. 2). The decadal data over the AS, BoB, and NIO basin suggests that the decade 2011–2020 shows a primary peak in the formation of tropical cyclones over AS whereas it is 1921–1930 for both BoB and NIO basin. Our results closely match the study by Mahala et al. (2015). The decades from 1981 to 2020 showed an increasing trend of tropical cyclones varying from 3 to 17 in the AS.

Table 4 depicts the statistics of tropical cyclones in the decades through 1891–2020 in the BoB and AS for EN, LN, pIOD, and nIOD years. The frequency of tropical cyclones during the decades is also computed for the EN, LN, pIOD, and nIOD years for the BoB and AS. The analysis suggests that during EN years, the BoB experiences 7.00 tropical cyclones in the decade 1941–1950 while it remains the same at 2.25 for the decades through 1991–2020. During LN years, the BoB experiences 7.00 tropical cyclones

**Table 3** Statistics of CS and SCS in the BoB, AS, and NIO basin during ENSO-IOD events from 1891 to 2020

Basin→	BoB		AS		NIO basin	
	CS	SCS	CS	SCS	CS	SCS
Events↓						
EN	77	70	15	33	92	103
LN	92	83	17	23	109	106
nENSO	118	84	22	23	140	107
pIOD	27	51	8	21	35	72
nIOD	59	37	9	15	68	52
noIOD	201	149	37	43	238	192

**Fig. 2** The decadal variability of the tropical cyclones in the BoB, AS, and NIO basin



**Table 4** Total number of tropical cyclones over the BoB and AS during EN/LN-pIOD/nIOD years in the decades through 1891–2020

Decades	LN		EN		pIOD		nIOD	
	BoB	AS	BoB	AS	BoB	AS	BoB	AS
1891–1900	25	4	13	1	-	-	20	3
1901–1910	25	5	11	6	-	-	22	5
1911–1920	7	1	14	1	-	-	8	3
1921–1930	11	1	19	2	11	0	7	0
1931–1940	14	3	6	2	-	-	7	1
1941–1950	13	0	7	1	-	-	5	0
1951–1960	11	0	4	3	-	-	16	5
1961–1970	8	5	21	4	12	5	4	3
1971–1980	19	8	16	4	12	3	-	-
1981–1990	18	1	10	1	12	1	-	-
1991–2000	12	5	9	3	8	2	7	4
2001–2010	5	4	9	6	7	3	-	-
2011–2020	7	3	9	13	16	15	-	-
Total	175	40	148	47	78	29	96	24

in the decade 1911–1920, and there is a decreasing trend in the tropical cyclone cases during the decades through 1971–2020. During pIOD years, BoB experiences a maximum frequency of 6.00 in the decade 1971–1980 and it follows a decreasing trend up to 2020, while the frequency is 7.00 each for the decades through 1921–1940 during nIOD years.

During EN years, the AS experienced a maximum of 3.25 tropical cyclones in the decade 2011–2020 while it is 2.50 during the LN years of the decade 1961–1970. The maximum frequency of tropical cyclones in the pIOD events of the decade 2011–2020 is noted as 2.14. The trend in the frequency of tropical cyclones is increasing during the EN/pIOD events of the decades from 1981 to 2020. The maximum frequency of tropical cyclones in the nIOD events of the decade 1961–1970 is 3.00, followed by 2.00 during 1991–2020. The study by Pathirana and Priyadarshani (2022) suggests that there is a warming trend of SST variability and a positive trend of DMI in the western tropical Indian Ocean favoring convective activity in the AS. The impact of ENSO on SST variability is higher in the AS than in the BoB. The higher frequency of tropical cyclones in the AS during EN/pIOD years may be attributed to the warmer SST variability and weakening of vertical wind shear.

### 3.3 Genesis of tropical cyclones

Genesis locations play an important role in the lifetime and intensity of tropical cyclones (Camargo et al. 2007b). The statistics on total number of the tropical cyclones in the BoB and AS during different ENSO-IOD events are presented in Table 5. A close inspection of the data reveals that a total of 53 (68) tropical cyclones have occurred in the BoB during the co-occurrence of the EN with pIOD

**Table 5** Number of tropical cyclones over BoB (AS) in different ENSO-IOD events

	EN	nENSO	LN	Total
nIOD	0 (0)	28 (12)	68 (12)	96 (24)
noIOD	95 (26)	160 (31)	95 (23)	350 (80)
pIOD	53 (21)	13 (3)	12 (5)	78 (29)
Total	148 (47)	201 (46)	175 (40)	524 (133)

The figures in the bracket denote the tropical cyclones over AS

(LN with nIOD) years. Similarly, a total of 21 (12) tropical cyclones have occurred in the AS during the co-occurrence of EN with pIOD (LN with nIOD) years. Concerning the relocation of the intertropical convergence zone (ITCZ), Mohanty (1994) claims that the genesis of cyclonic disturbances over the BoB can drastically vary in a latitudinal direction from 5° N to 20° N. Based on this fact, the BoB is equally divided into three regions: (i) southern (5–10° N) ( $R_1$ ), (ii) central (10–15° N) ( $R_2$ ), and (iii) northern (15–20° N) ( $R_3$ ). Figure 3 shows the genesis locations of tropical cyclones in each region under different ENSO and IOD events. During EN and LN years, the maximum (minimum) number of tropical cyclones are formed in  $R_2$  ( $R_3$ ) while in nENSO years, the maximum (minimum) number of tropical cyclones are formed in  $R_1$  ( $R_3$ ). The results indicate that the peak density in the genesis locations is observed in  $R_2$  compared with other regions in various ENSO regimes. Moreover, the genesis of tropical cyclones in the IOD years shows that the maximum number of tropical cyclones is formed in both  $R_2$  and  $R_3$  during nIOD years while it is  $R_2$  during pIOD years. During noIOD years, the maximum (minimum) number of tropical cyclones is formed in  $R_1$ ( $R_3$ ).

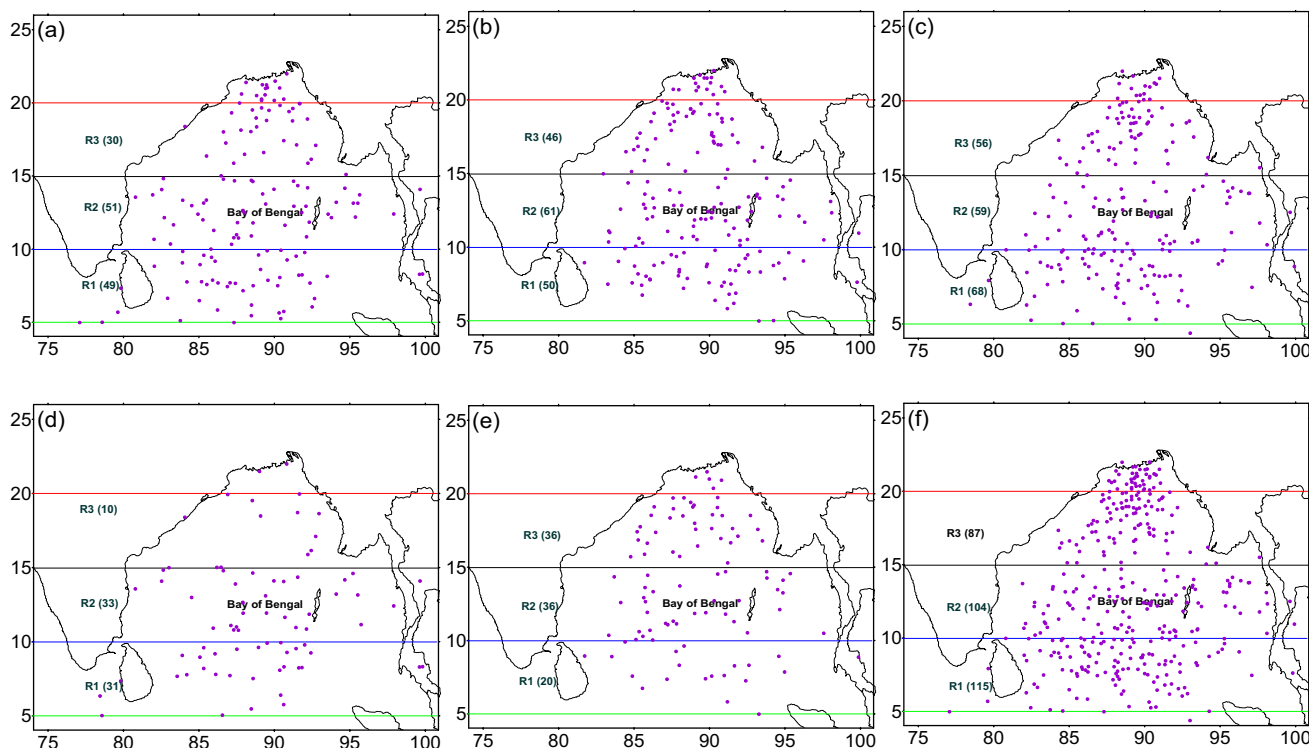


**Fig. 3** Genesis locations of tropical cyclones during the ENSO-IOD events during 1891–2020 **a** EN, **b** LN, **c** nENSO, **d** pIOD, **e** nIOD, **f** noIOD. The number within the bracket indicates the number of tropical cyclones formed in the regions

In addition, AS is divided into four specific regions: (i) AS1 (5–10 °N), (ii) AS2 (10–15° N), (iii) AS3 (15–20° N), (iv) AS4 (20–25° N). The genesis locations of tropical cyclones over AS in each region are computed and presented in Table 6. During the ENSO, pIOD, and noIOD years, the maximum (minimum) number of tropical cyclone cases is observed in the AS2 (AS4) region. However, the AS2 and AS3 regions experience maximum tropical cyclone cases during nIOD years. Our results are in good agreement with the study by Pathirana and Priyadarshani (2022). The analysis indicates that the genesis locations of tropical cyclones over AS are the highest in the AS2 region. In general, the magnitude of surface winds in the AS and the BoB is strong in August and February (Duan et al. 2021) which in turn induces a cooling effect that leads to a bimodal seasonal cycle of the SST. As a result, the SST in the region 5–15° N (10–20° N) of the AS (BoB) exceeds 30 °C in May, and

28 °C in November. These provide a favorable oceanic condition for tropical cyclone genesis in the region 10–15° N. Also, both AS and BoB possess relatively low vertical wind shear of around 10 m/s in May and November in the region 5–20° N, which is conducive for tropical cyclone genesis.

We have computed the genesis locations of tropical cyclones in the regions 5–10° N, 10–15° N, 15–20° N, and 20–25° N in both the BoB and AS (Fig. 4). The analysis indicates that the number of BoB tropical cyclones in the region 10–15° N is more than in 5–10° N during the decades through 1981–2010 and a reverse pattern in the decade 2011–2020 (Fig. 4a). Similarly, the region 10–15° N shows an increasing trend in the genesis of tropical cyclones in the decades through 1971–2020 in the AS (Fig. 4b). However, a variability in the genesis locations of the BoB and AS tropical cyclones is distinctly observed in the decades through 1891–2020.

**Table 6** Genesis of tropical cyclones over the AS during different ENSO-IOD events

Region	EN	LN	nENSO	pIOD	nIOD	noIOD
AS1 (05–10° N)	12	8	8	7	5	16
AS2 (10–15° N)	24	22	22	15	9	44
AS3 (15–20° N)	10	8	14	6	9	17
AS4 (20–25° N)	1	2	2	1	1	3



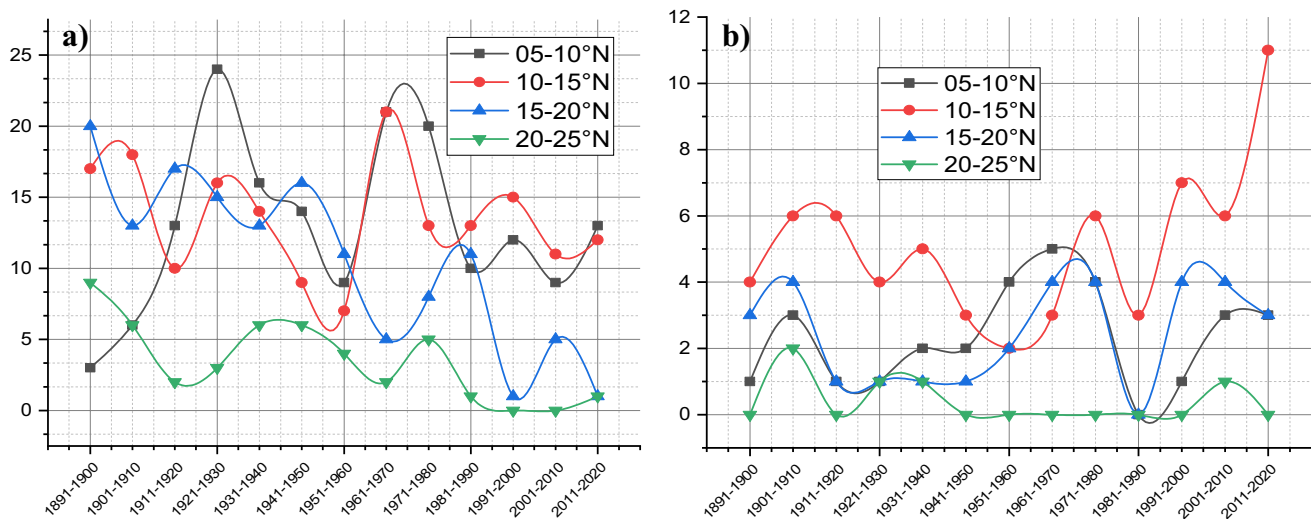


**Fig. 4** Decadal variability of the tropical cyclones in the regions 5–10° N, 10–15° N, 15–20° N, and 20–25° N in BoB (a), AS (b). The x-axis denotes decades and the y-axis denotes the total number of tropical cyclones

In addition, we have computed the number of tropical cyclones over the BoB and AS during the pre-monsoon (Mar–Apr–May) and post-monsoon (Oct–Nov–Dec) seasons. It is observed that the number of tropical cyclones in the post-monsoon season is more than that of the pre-monsoon season, accounting for 71.55% of the total number of tropical cyclones formed in the pre- and post-monsoon seasons. The average lifetime (in days) of the BoB tropical cyclones in LN (EN) years is 5.03 (5.21) while it is 5.63 (6.72) for the AS tropical cyclones. However, the study by Mahala et al. (2015) indicated that the average lifetime of BoB tropical cyclones in the LN (EN) is 5.13 (4.89) and their study period is 1891–2007. The average lifetime of tropical cyclones for the period 2008–2020 in the BoB is computed as 6.40 (7.16) in LN (EN) years while it is 7.00 (9.21) for the AS. The analysis suggests that the average lifetime of tropical cyclones in both the BoB and AS is increasing during the EN/LN years after 2007.

### 3.4 Wavelet coherence between frequency of tropical cyclones and climate forcings

WTC is a method for analyzing the phase lag and coherence of two-time series as a function of frequency and time (Chang and Glover 2010). This approach has proven to be the most efficient way to reveal climate links between two independent time series. The relationship between the frequency of tropical cyclones and climate forcings is studied using the WTC method. The level of statistical significance of WTC is measured using the Monte Carlo method (Ng and Chan 2012). The coherence ranges from 0 to 1. In this study, Monte Carlo WTC analysis is used to quantify the linkage between tropical cyclones frequency and climate forcings (ENSO/IOD) in the NIO basin, BoB and AS. Figure 5 shows the WTC between

the frequency of tropical cyclones and DMI/ Niño 3.4 indices. Arrows in the regions of high WTC indicate the phase relationship between the two parameters. Two cross-wavelet parameters in the regions are in phase (not-in-phase) if the arrows point right (left) region and the leading (lagging) is represented by arrows pointing upwards (downwards). Vectors are drawn only for regions where the squared coherence is either greater than or equal to 0.5. A solid grey line is used to depict the cone of influence (COI) in which the edge effect becomes significant at different frequencies and the 95% significant region of confidence level is delimited by a solid black line.

In the NIO basin, a strong WTC between tropical cyclone frequency and DMI (Fig. 5a) is observed from 1951 to 1960 at the period band of 10–16 months followed by 1960 to 1964 over a period of about 16–32 months. During these periods, both the parameters are not-in-phase and the frequency of tropical cyclones leads. Moreover, the years from 2006 to 2020 at a period band of about 134 months show high WTC, and arrows pointing right indicate a significant relationship between the parameters. Considering the WTC between the frequency of NIO tropical cyclones and Niño 3.4 index (Fig. 5b), it is observed that the period from 1938 to 1946 shows that these two parameters are in-phase at a period band of 40–52 months where Niño 3.4 index leads. The years from 1891 to 1896 show high WTC at a period of the band of about 64 months, during which the parameters are not-in-phase. The period 2006–2020 shows high WTC at a period band of about 160 months, during which the parameters are not-in-phase and Niño 3.4 index leads. Moreover, a high WTC is observed in the period 1991–2020 at a period band of about 256–350 months, during which the parameters are not-in-phase and the frequency leads for a quarter of the ENSO cycle.

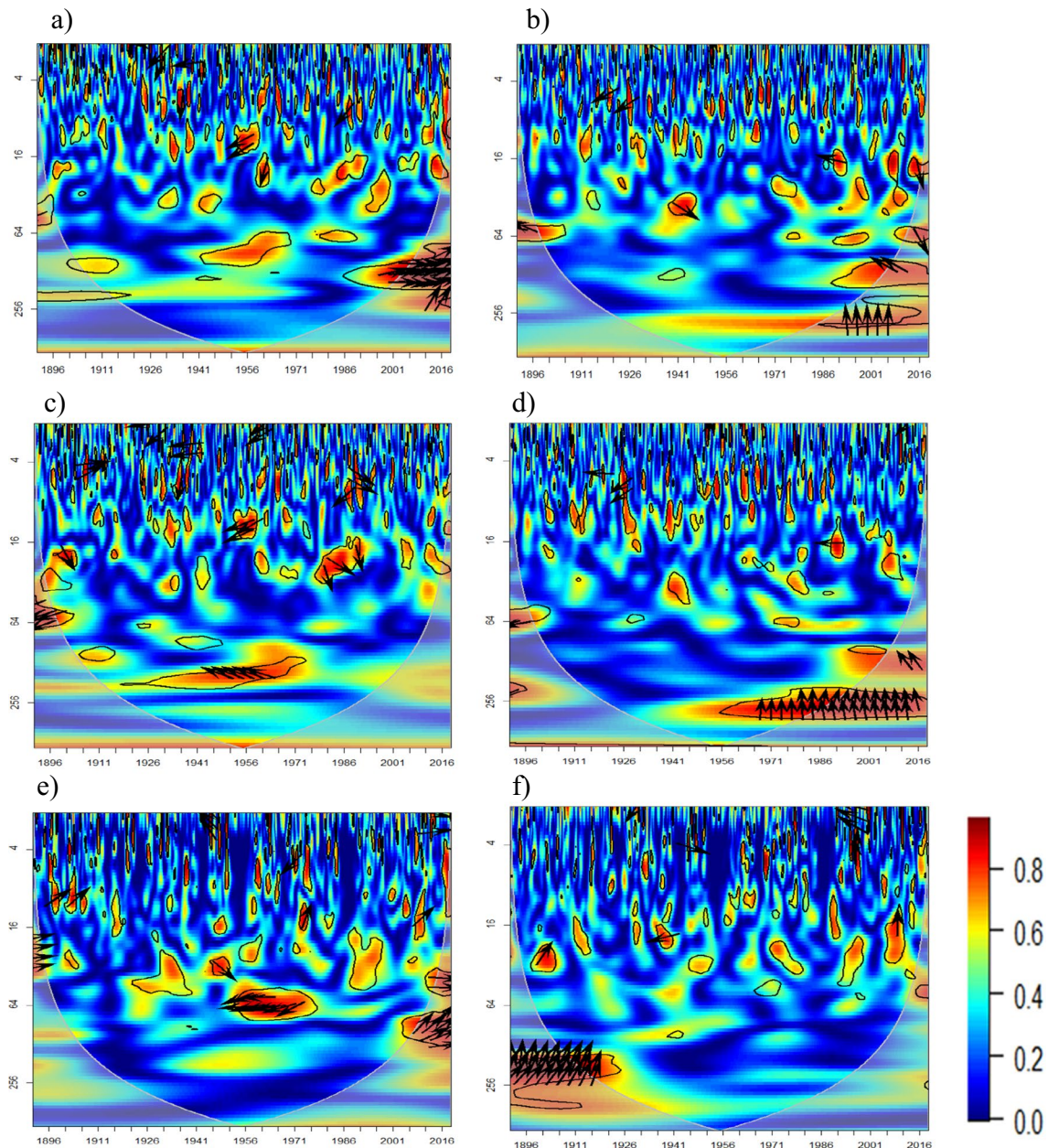


**Fig. 5** Wavelet coherence between frequency of **a** NIO tropical cyclones and DMI, **b** NIO tropical cyclones and Niño 3.4 index, **c** BoB tropical cyclones and DMI, **d** BoB tropical cyclones and Niño 3.4 index, **e** AS tropical cyclones and DMI, and **f** AS tropical cyclones and Niño 3.4 index during 1891–2020. The phase relation-

ship is represented by arrows. The black solid line contour delimits the region (red) where the power is strong and significant, and the cone of influence (grey line) indicates the 95% confidence level. The  $x$ -axis denotes year and the  $y$ -axis denotes scale in months

Figure 5c shows the wavelet coherence between frequency of BoB tropical cyclones and DMI. A high WTC is observed between tropical cyclones frequency and DMI, for the period 1951–1960 at a period band of 12–16 months, during which both the parameters are not-in-phase and frequency leads. The years from 1896 to 1904 show the high WTC, and the parameters are in-phase at a period band of about 16–24 months, during which DMI leads. Also, the period from

1891 to 1896 (1921–1973) delineates a high coherence at the period band of about 60–66 (208) months, during which the parameters are not-in-phase. The frequency of tropical cyclones (DMI) leads in the period 1891–1896 (1921–1973). The period from 1976 to 1991 at a period band of 16–40 months shows a high coherence with the parameters in-phase and DMI leads. During ENSO years, high coherence is observed during 1926–1930 (1989–1994) at a period band

of about 4–16 (16–24) months, during which both the parameters are not-in-phase and the frequency of tropical cyclones leads (Fig. 5d). There is a phase lag of almost a quarter of a cycle (6 to 21 months) between Niño 3.4 index and the frequency of tropical cyclones at a period band of around 256 months during 1956–1986 and 1991–2020.

In the AS, high WTC between DMI and frequency of tropical cyclones is noted during 1953–1976 at a period band of around 64 months, in which both the parameters are not-in-phase (Fig. 5e). The effect is delayed by approximately half a cycle. Furthermore, the years from 2010 to 2020 at a period band of around 112 months show that both parameters are in-phase with frequency leads. Also, Niño 3.4 index and the frequency of tropical cyclones are in-phase during 1891–1910 at a period band of 208 months, in which the frequency of tropical cyclones leads (Fig. 5f).

The influence of DMI and Niño 3.4 index on the frequency of tropical cyclones for an interannual scale (16 months) seems weak as shown by various patch sizes of high coherence in different years. Generally, some of the specific years as discussed above may be associated with ENSO and IOD events in the tropical Indian Ocean (Ashok et al. 2003; Nur'utami and Hidayat 2016; Saji et al. 1999). The analysis indicates that AS tropical cyclones are influenced by DMI in the decade 2011–2020. Furthermore, DMI provides a useful indication of the post-monsoon tropical cyclone genesis in advance, which could be a potential tool in forecasting tropical cyclones in the years with DMI leads (Singh 2008).

Under certain circumstances, there may be a weak link between the frequency of tropical cyclones and Niño 3.4/DMI. Therefore, the dependency and coherence between the frequency of tropical cyclones and climate forcings have been determined using multiple linear regression. For multiple linear regression, the explanatory variables Niño 3.4 and DMI are utilized. The results of the multiple linear regression statistical analysis of the frequency of tropical cyclones and the independent variables are displayed in Table 7. The *t*-values and *p*-values are both important in multiple linear regression to assess the statistical significance of the regression coefficients and determine whether the predictable variable is associated with the outcome variable. The greater the magnitude of *t*, the greater the evidence to reject the null hypothesis. A *p*-value of more than 0.05 implies that

the null hypothesis is true. Conventionally, a *p*-value less than 0.05 is referred to as statistically significant, and less than 0.001 is highly significant (Chatterjee and Simonoff 2013). The results show a significant correlation (*p*-value of 0.0133) between the frequency of tropical cyclones and the DMI. The *p*-value (0.6120) of the Niño 3.4 index shows an insignificant association with the frequency of tropical cyclones as it is much more than 0.05.

The teleconnection between climate forcings and the frequency of tropical cyclones in the NIO basin seems to be statistically significant for the DMI while it is insignificant for the Niño 3.4 index. Our results are supported by the findings of the study by Soulard et al. (2019) which claims the location of SSTA related to ENSO and the mean zonal flow in the tropical Pacific sets up Rossby-waves that propagate into mid-latitudes. Any change associated with any of these conditions has the potential to alter the teleconnection between ENSO and the extra-tropical Northern Hemisphere. Also, the relative frequency of east Pacific and the central Pacific events may change due to the warming of global oceans as a result of which SST change will be patterned and not uniform. Studies by Kao and Yu 2009, McPhaden 2012, Hu et al. 2013, Lübbecke and McPhaden 2014, Yeh et al. 2015, and Guan and McPhaden 2016 suggest that SSTA location is shifting towards the central Pacific, which further suggests that central Pacific events should become more frequent. This would result in a weak relationship between ENSO and the tropical Northern Hemisphere events, while the ENSO-Pacific North American relationship will be stronger.

### 3.5 Wavelet coherence between Niño 3.4 index and DMI

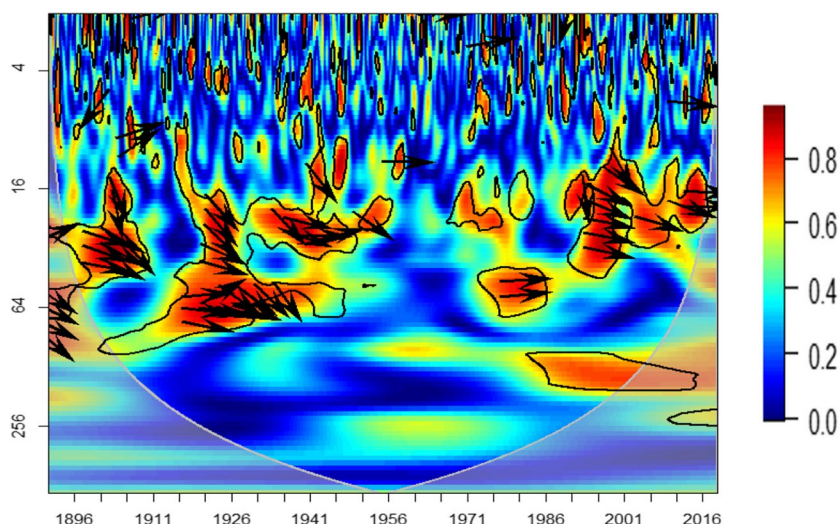
In this section, the WTC method is used to know the possible teleconnection between ENSO and IOD for the period 1891–2020. Figure 6 shows the coherence analysis between Niño 3.4 index and DMI. The arrows pointing to the right indicate the parameters are in-phase suggesting both Niño 3.4 and DMI reach their maximum peaks during certain periods. The analysis shows that the co-occurrence of both events happen in the same calendar year and it is in agreement with the study by Isa et al. (2020). It is also crucial to observe that the time series shows a distinct appearance of periods that are fewer than 13 months, with different phase connections between the DMI and Niño 3.4 index. A high coherency between Niño 3.4 and DMI is observed with an interannual time scale of 16–64 months during the periods 1896–1910, 1916–1956, 1975–1986, and 1991–2015. The study by Maruyama et al. (2011) suggests that before a regime shift, there is a high coherence between Niño 3.4 and DMI, which is evident in the period 1976–1985 showing a high coherency followed by a shift to the period 1986–2015. During 1976–1985, the climate forcings are in-phase. Less significant coherence between Niño 3.4 and DMI for the

**Table 7** The output of the multiple linear regression model in which frequency of tropical cyclones is a dependent variable and Niño 3.4, DMI are independent variables

Variables	Estimate	Std. Error	<i>t</i> -value	<i>p</i> -value	Significance
DMI	-0.12923	0.05215	-2.478	0.0133	*
Niño 3.4	-0.01187	0.02341	-0.507	0.6120	

Significance code: 0 '\*\*\*\*' 0.001 '\*\*\*' 0.01 '\*\*' 0.05 '.' 0.1 '.'1

**Fig. 6** Wavelet coherence between Niño 3.4 and DMI during 1891–2020. The white transparent area indicates the region inside the COI (cone of influence) and the thick black contour signifies a 95% confidence level. The phase relationship is represented by arrows. The *x*-axis denotes years and the *y*-axis denotes scale in months



period 1958–1965 indicates that IOD and ENSO are not related, which is consistent with the study by Ashok et al. (2003). The years 1976 and 1997 show a strong EN with pIOD event, during which a high coherence of more than 0.7 is noted. This may be attributed to the atmospheric bridge connecting ENSO with the Indian Ocean during the evolution of the pIOD. Apparently, for the period 1991–2001, high coherence between Niño 3.4 index and DMI can be attributed to the interaction of Pacific events with the Indian Ocean through the atmospheric bridge as reported by earlier studies (Ashok et al. 2003; Ueda and Matsumoto 2000).

We have computed the frequency of tropical cyclones in the NIO basin for the years 1896–1910, 1916–1956, 1975–1986, and 1991–2015 for the EN, LN, pIOD, nIOD, the co-occurrences EN-pIOD, and LN-nIOD events. It is observed that the period 1916–1956 shows the highest frequency of 6.5 in EN events. In LN events, the period 1896–1910 shows the highest frequency of 6, followed by 5 during the period 1975–1986. In addition, the highest frequency of 5.67 is noted in the pIOD (nIOD) events of 1975–1986 (1896–1910). In the period 1916–1956, the highest frequency of 5.5 is noted in the co-occurrence of EN with pIOD, following a decreasing trend in the subsequent years. Furthermore, during the co-occurrence of LN with nIOD, the period 1896–1910 shows the highest frequency, followed by 1916–1956. In addition, no cases are recorded after 1975.

## 4 Conclusions

The study establishes the impacts of low-frequency climate variabilities such as ENSO and IOD events on tropical cyclone activities in the NIO basin consisting of both the

BoB and the AS for the period 1891–2020. The climatological mean for the frequency of tropical cyclones in the NIO basin, BoB, and the AS are computed as 5.05, 4.03, and 1.02, respectively, for the period 1891–2020. The study suggests that the primary peak in the genesis of tropical cyclones in the NIO basin is 1921–1930, and the frequency is higher during EN years and nIOD years. In the BoB (AS), the frequency is higher during LN (EN) and nIOD (pIOD) years. The decade 1921–1930 (2011–2020) shows a primary peak for the genesis of tropical cyclones over the BoB (AS). In the BoB, the decades through 1971–2020 show a decreasing trend in the genesis of tropical cyclones during LN years while the decades through 1981–2020 show a decreasing trend during pIOD years. The higher frequency of tropical cyclones in the AS during EN/pIOD years is attributed to the warmer SST variability and weakening of vertical wind shear.

The genesis locations of BoB and AS tropical cyclones reveal that the peak density is observed in the belt 10–15° N over BoB and AS during ENSO and IOD years while the genesis is higher over the belt 15–20° N over AS during nIOD years. Higher SST and lower vertical wind shear over 10–15° N are attributed to the peak density. Tropical cyclone over the BoB and AS has higher frequency during pre-monsoon and post-monsoon seasons and accounts for 71.55% of the total tropical cyclones formed in the pre- and post-monsoon seasons.

The average lifetime (in days) for the BoB tropical cyclones in LN (EN) years is 5.03 (5.21) while it is 5.63 (6.72) for the AS tropical cyclones. However, the lifetime of tropical cyclones from 2008 to 2020 shows an increasing trend; 6.40 (7.16) during LN (EN) years over BoB and 7.00 (9.21) over AS.

WTC of the frequency of tropical cyclones over the NIO basin with DMI and Niño 3.4 index indicates high coherence and the in-phase relationship between DMI and frequency for the period 2006–2020 while the out-of-phase relationship with Niño 3.4 index has high coherence. However, WTC of frequency of tropical cyclones with DMI over BoB (AS) separately shows higher coherence during 1921–1973 (1953–1976) but out-of-phase relationship. On the other hand, the periods 1956–1986 and 1991–2020 show high coherence with a phase lag of around a quarter of a cycle between the frequency of tropical cyclones and the Niño 3.4 index for the BoB, while it is 1891–1910 for the AS.

The multiple linear regression analysis shows a significant (insignificant) correlation between the frequency and DMI (Niño 3.4 index) of tropical cyclones over the NIO basin. The years 1976 and 1997 having co-occurrence of a strong EN with pIOD event show high coherence of more than 0.7. This may be attributed to the atmospheric bridge that connects ENSO with the Indian Ocean in the evolution of the pIOD. In addition, during 1991–2001, a high coherence between Niño 3.4 index and DMI may be attributed to the interaction of Pacific events with the Indian Ocean through an atmospheric bridge.

Though the annual frequency of tropical cyclones in the BoB is significantly higher than over AS, the increasing trend in the frequency of tropical cyclones in the AS during the decade 2011–2020 is a matter of concern and provides scope for future investigations on various influencing factors on tropical cyclone genesis and track position. The limitation of the present study is the use of the data prior to the satellite era.

**Acknowledgements** The encouragement received from the Kalinga Institute of Industrial Technology (KIIT) Deemed to be University, Odisha, India for doing this research work is gratefully acknowledged. The authors are also thankful to the India Meteorological Department for the database cyclone e-Atlas (version-2.0/2011)

**Author contribution** K. L. Xalxo: downloaded the data, compiled the codes, prepared the graphics, and tables, and wrote the manuscript. B. K. Mahala: designed the problem, analyzed the data, and co-wrote the paper. P. K. Mohanty: discussed and analyzed, co-wrote, and reviewed the paper.

A. Routray: analyzed, co-wrote, and reviewed the paper. S. Mohanty: reviewed the paper.

**Data availability** The datasets used and analyzed during the current study are available in the following repositories: i) <https://14.139.191.203/AboutEAtlas.aspx> ii) [https://psl.noaa.gov/gcos\\_wgsp/Timeseries/Data/nino34.long.anom.data](https://psl.noaa.gov/gcos_wgsp/Timeseries/Data/nino34.long.anom.data) iii) [https://psl.noaa.gov/gcos\\_wgsp/Timeseries/Data/dmi.had.long.data](https://psl.noaa.gov/gcos_wgsp/Timeseries/Data/dmi.had.long.data) iv) <https://climatedataguide.ucar.edu/climate-data/nino-sst-indices-nino-12-3-34-4-oni-and-tni> v) [https://origin.cpc.ncep.noaa.gov/products/analysis\\_monitoring/ensostuff/ONI\\_v5.php](https://origin.cpc.ncep.noaa.gov/products/analysis_monitoring/ensostuff/ONI_v5.php)

## Declarations

**Competing interests** The authors declare no competing interests.

## References

- Aguiar-Conraria L, Soares MJ (2014) The continuous wavelet transform: moving beyond uni- and bivariate analysis. *J Econ Surv* 28:344–375
- Ashok K, Behera SK, Rao SA et al (2007) El Niño Modoki and its possible teleconnection. *J Geophys Res Oceans* 112:1–27. <https://doi.org/10.1029/2006JC003798>
- Ashok K, Guan Z, Yamagata T (2001) Impact of the Indian Ocean dipole on the relationship between the Indian monsoon rainfall and ENSO. *Geophys Res Lett* 28:4499–4502. <https://doi.org/10.1029/2001GL013294>
- Ashok K, Guan Z, Yamagata T (2003) A look at the relationship between the ENSO and the Indian Ocean Dipole. *J Meteorol Soc Jpn* 81:41–56. <https://doi.org/10.2151/jmsj.81.41>
- Bhardwaj P, Pattanaik DR, Singh O (2019) Tropical cyclone activity over Bay of Bengal in relation to El Niño–Southern Oscillation. *Int J Climatol* 39:5452–5469. <https://doi.org/10.1002/joc.6165>
- Cai W, Cowan T (2008) Dynamics of late autumn rainfall reduction over southeastern Australia. *Geophys Res Lett* 35:1–5. <https://doi.org/10.1029/2008GL033727>
- Camargo SJ, Emanuel KA, Sobel AH (2007a) Use of a genesis potential index to diagnose ENSO effects on tropical cyclone genesis. *J Clim* 20:4819–4834. <https://doi.org/10.1175/JCLI4282.1>
- Camargo SJ, Robertson AW, Gaffney SJ et al (2007b) Cluster analysis of typhoon tracks. Part I: General properties. *J Clim* 20:3635–3653. <https://doi.org/10.1175/JCLI4188.1>
- Camargo SJ, Robertson AW, Gaffney SJ et al (2007c) Cluster analysis of typhoon tracks. Part II: Large-scale circulation and ENSO. *J Clim* 20:3654–3676. <https://doi.org/10.1175/JCLI4203.1>
- Camargo SJ, Sobel AH (2005) Western North Pacific tropical cyclone intensity and ENSO. *J Clim* 18:2996–3006. <https://doi.org/10.1175/JCLI3457.1>
- Capotondi A, Wittenberg AT, Newman M et al (2015) Understanding ENSO diversity. *Bull Am Meteorol Soc* 96:921–938. <https://doi.org/10.1175/BAMS-D-13-00117.1>
- Chan JCL (2007) Interannual variations of intense typhoon activity. *Tellus Ser A Dyn Meteorol Oceanogr* 59:455–460. <https://doi.org/10.1111/j.1600-0870.2007.00241.x>
- Chang C, Glover GH (2010) Time-frequency dynamics of resting-state brain connectivity measured with fMRI. *NeuroImage* 50:81–98. <https://doi.org/10.1016/j.neuroimage.2009.12.011>
- Chang X, Wang B, Yan Y et al (2019) Characterizing effects of monsoons and climate teleconnections on precipitation in China using wavelet coherence and global coherence. *Clim Dyn* 52:5213–5228
- Chatterjee S, Simonoff JS (2013) *Handbook of regression analysis*. John Wiley & Sons, Inc., Hoboken. <https://onlinelibrary.wiley.com/doi/book/10.1002/9781118532843>
- Chen D, Lian T, Fu C et al (2015) Strong influence of westerly wind bursts on El Niño diversity. *Nat Geosci* 8:339–345. <https://doi.org/10.1038/ngeo2399>
- Chia HH, Ropelewski CF (2002) The interannual variability in the genesis location of tropical cyclones in the northwest Pacific. *J Clim* 15:2934–2944. [https://doi.org/10.1175/1520-0442\(2002\)015<2934:TIVITG>2.0.CO;2](https://doi.org/10.1175/1520-0442(2002)015<2934:TIVITG>2.0.CO;2)
- Chui CK (1992) *An introduction to wavelets*. Academic Press, San Diego
- Du Y, Cai W, Wu Y (2013) A New Type of the Indian Ocean Dipole since the mid-1970s. *J Clim* 26:959–972. <https://doi.org/10.1175/JCLI-D-12-00047.1>
- Duan W, Yuan J, Duan X, Feng D (2021) Seasonal variation of tropical cyclone genesis and the related large-scale environments: Comparison between the Bay of Bengal and Arabian sea sub-basins. *Atmosphere* 12. <https://doi.org/10.3390/atmos12121593>

- Fan L, Liu Q, Wang C, Guo F (2017) Indian Ocean Dipole modes associated with different types of ENSO development. *J Clim* 30:2233–2249. <https://doi.org/10.1175/JCLI-D-16-0426.1>
- Gabor D (1946) Theory of communication. *J Inst Electr Eng* 93:429–457
- Girishkumar MS, Ravichandran M (2012) The influences of ENSO on tropical cyclone activity in the Bay of Bengal during October–December. *J Geophys Res Oceans* 117:1–13. <https://doi.org/10.1029/2011JC007417>
- Grimm AM, Barros VR, Doyle ME (2000) Climate variability in southern South America associated with El Niño and La Niña events. *J Clim* 13:35–58. [https://doi.org/10.1175/1520-0442\(2000\)013<0035:CVISSA>2.0.CO;2](https://doi.org/10.1175/1520-0442(2000)013<0035:CVISSA>2.0.CO;2)
- Grinsted A, Moore JC, Jevrejeva S (2004) Application of the cross wavelet transform and wavelet coherence to geophysical time series. *Nonlinear Process Geophys* 11:561–566. <https://doi.org/10.5194/npg-11-561-2004>
- Guan C, McPhaden MJ (2016) Ocean processes affecting the twenty-first-century shift in ENSO SST variability. *J Clim* 29:6861–6879. <https://doi.org/10.1175/JCLI-D-15-0870.1>
- Hong CC, Lu MM, Kanamitsu M (2008) Temporal and spatial characteristics of positive and negative Indian Ocean dipole with and without ENSO. *J Geophys Res Atmos* 113:1–15. <https://doi.org/10.1029/2007JD009151>
- Hu ZZ, Kumar A, Ren HL et al (2013) Weakened interannual variability in the tropical Pacific ocean since 2000. *J Clim* 26:2601–2613. <https://doi.org/10.1175/JCLI-D-12-00265.1>
- Hudgins L, Friehe CA, Mayer ME (1993) Wavelet transforms and atmospheric turbulence. *Phys Rev Lett* 71:3279
- Isa NS, Akhir MF, Kok PH et al (2020) Spatial and temporal variability of sea surface temperature during El-Niño Southern Oscillation and Indian Ocean Dipole in the Strait of Malacca and Andaman Sea. *Reg Stud Mar Sci* 39:101402. <https://doi.org/10.1016/j.risma.2020.101402>
- Islam Z (2018) Classification of el niño and la niña years for water resources management in alberta. *Can J Civ Eng* 45:1093–1098
- Kao HY, Yu JY (2009) Contrasting Eastern-Pacific and Central-Pacific types of ENSO. *J Clim* 22:615–632. <https://doi.org/10.1175/2008JCLI2309.1>
- Kranthi GM, Deshpande M, Sunilkumar K et al (2023) Climatology and characteristics of rapidly intensifying tropical cyclones over the North Indian Ocean. *Int J Climatol* 43:1773–1795. <https://doi.org/10.1002/joc.7945>
- Lau KM, Weng H (1995) Climate signal detection using wavelet transform: how to make a time series sing. *Bull Am Meteorol Soc* 76:2391–2402. [https://doi.org/10.1175/1520-0477\(1995\)076<2391:CSDUWT>2.0.CO;2](https://doi.org/10.1175/1520-0477(1995)076<2391:CSDUWT>2.0.CO;2)
- Lestari RK, Koh TY (2016) Statistical evidence for asymmetry in ENSO–IOD interactions. *Atmos Ocean* 54:498–504. <https://doi.org/10.1080/07055900.2016.1211084>
- Liu KS, Chan JCL (2003) Climatological characteristics and seasonal forecasting of tropical cyclones making landfall along the South China Coast. *Mon Weather Rev* 131:1650–1662. <https://doi.org/10.1175/2554.1>
- Lübbecke JF, McPhaden MJ (2014) Assessing the twenty-first-century shift in ENSO variability in terms of the Bjerknes stability index. *J Clim* 27:2577–2587. <https://doi.org/10.1175/JCLI-D-13-00438.1>
- Mahala BK, Nayak BK, Mohanty PK (2015) Impacts of ENSO and IOD on tropical cyclone activity in the Bay of Bengal. *Nat Hazards* 75:1105–1125. <https://doi.org/10.1007/s11069-014-1360-8>
- Maraun D, Kurths J (2004) Cross wavelet analysis: significance testing and pitfalls. *Nonlinear Process Geophys* 11:505–514
- Maruyama F, Kai K, Morimoto H (2011) Wavelet-based multifractal analysis of the El Niño/Southern Oscillation, the Indian Ocean Dipole and the North Atlantic oscillation. *Sci Online Lett* 7:65–68. <https://doi.org/10.2151/sola.2011-017>
- McKenna S, Santoso A, Sen GA et al (2020) Indian Ocean Dipole in CMIP5 and CMIP6: characteristics, biases, and links to ENSO. *Sci Rep* 10:1–13. <https://doi.org/10.1038/s41598-020-68268-9>
- McPhaden MJ (2004) Evolution of the 2002/03 El Niño. *Bull Am Meteorol Soc* 85:677–695. <https://doi.org/10.1175/BAMS-85-5-677>
- McPhaden MJ (2012) A 21st century shift in the relationship between ENSO SST and warm water volume anomalies. *Geophys Res Lett* 39:1–5. <https://doi.org/10.1029/2012GL051826>
- Meyers G, McIntosh P, Pigot L, Pook M (2007) The years of El Niño, La Niña and interactions with the tropical Indian Ocean. *J Clim* 20:2872–2880. <https://doi.org/10.1175/JCLI4152.1>
- Mohanty UC (1994) Tropical cyclones in the Bay of Bengal and deterministic methods for prediction of their trajectories. *Sadhana* 19:567–582
- Mohanty UC, Osuri KK, Pattanayak S, Sinha P (2012) An observational perspective on tropical cyclone activity over Indian seas in a warming environment. *Nat Hazards* 63:1319–1335. <https://doi.org/10.1007/s11069-011-9810-z>
- Mostafa F (2020) Multiple linear regression, its statistical analysis and application in energy efficiency, pp 1–26. <https://doi.org/10.20944/preprints202010.0082.v1>
- Murtugudde R, McCreary JP, Busalacchi AJ (2000) Oceanic processes associated with anomalous events in the Indian Ocean with relevance to 1997–1998. *J Geophys Res Oceans* 105:3295–3306. <https://doi.org/10.1029/1999jc900294>
- Ng EKW, Chan JCL (2012) Geophysical applications of partial wavelet coherence and multiple wavelet coherence, pp 1845–1853. <https://doi.org/10.1175/JTECH-D-12-00056.1>
- Nur'utami MN, Hidayat R (2016) Influences of IOD and ENSO to Indonesian rainfall variability: role of atmosphere–ocean interaction in the Indo-Pacific sector. *Procedia Environ Sci* 33:196–203. <https://doi.org/10.1016/j.proenv.2016.03.070>
- Pathirana G, Priyadarshani K (2022) Tropical cyclones in the Arabian Sea and the Bay of Bengal: comparison of environmental factors. *J Natl Sci Found Sri Lanka* 50:53–64. <https://doi.org/10.4038/jnsfr.v50i1.10424>
- Power K, Axelsson J, Wangdi N, Zhang Q (2021) Regional and local impacts of the ENSO and IOD events of 2015 and 2016 on the Indian summer monsoon—a Bhutan case study. *Atmosphere* 12. <https://doi.org/10.3390/atmos12080954>
- Roose S, Ajayamohan RS, Ray P et al (2022) ENSO influence on Bay of Bengal cyclogenesis confined to low latitudes. *NPJ Clim Atmos Sci* 5. <https://doi.org/10.1038/s41612-022-00252-8>
- RSMC (Regional Specialised Meteorological Centre - Indian Meteorological Department) (2011) Tracks of cyclones and depressions over North Indian Ocean, Cyclone eAtlas – IMD, Version 2.0 / 2011. Chennai
- Saji NH, Goswami PN, Vinayachandran PN, Yamagata T, Saji NA et al (1999) Dipole mode in the tropical Indian ocean. *Nature* 401:360–363
- Santoso A, England MH, Cai W (2012) Impact of Indo-Pacific feedback interactions on ENSO dynamics diagnosed using ensemble climate simulations. *J Clim* 25:7743–7763. <https://doi.org/10.1175/JCLI-D-11-00287.1>
- Saunders MA, Chandler RE, Merchant CJ, Roberts FP (2000) Atlantic hurricanes and NW Pacific typhoons: ENSO spatial impacts on occurrence and landfall. *Geophys Res Lett* 27:1147–1150
- Schulte JA, Najjar RG, Li M (2016) The influence of climate modes on streamflow in the mid-Atlantic region of the United States. *J Hydrol: Reg Stud* 5:80–99
- Singh A, Delcroix T, Cravatte S (2011) Contrasting the flavors of El Niño–Southern Oscillation using sea surface salinity observations. *J Geophys Res Oceans* 116:1–16. <https://doi.org/10.1029/2010JC006862>
- Singh OP (2008) Indian Ocean dipole mode and tropical cyclone frequency. *Curr Sci* 94:29–31

- Singh OP, Ali Khan TM, Rahman MS (2000) Changes in the frequency of tropical cyclones over the North Indian Ocean. *Meteorog Atmos Phys* 75:11–20. <https://doi.org/10.1007/s007030070011>
- Singh OP, Ali Khan TM, Sazedur Rahman M (2001) Probable reasons for enhanced cyclogenesis in the Bay of Bengal during July–August of ENSO years. *Glob Planet Chang* 29:135–147. [https://doi.org/10.1016/S0921-8181\(00\)00090-4](https://doi.org/10.1016/S0921-8181(00)00090-4)
- Singh VK, Roxy MK (2022) A review of ocean-atmosphere interactions during tropical cyclones in the north Indian Ocean. *Earth Sci Rev* 226:103967. <https://doi.org/10.1016/j.earscirev.2022.103967>
- Soulard N, Lin H, Yu B (2019) The changing relationship between ENSO and its extratropical response patterns. *Sci Rep* 9:1–10. <https://doi.org/10.1038/s41598-019-42922-3>
- Sreelekha PN, Babu CA (2019) Is the negative IOD during 2016 the reason for monsoon failure over southwest peninsular India? *Meteorog Atmos Phys* 131:413–420. <https://doi.org/10.1007/s00703-017-0574-1>
- Sun S, Lan J, Yue Fang T, Gao X (2015) A triggering mechanism for the Indian Ocean dipoles independent of ENSO. *J Clim* 28:5063–5076. <https://doi.org/10.1175/JCLI-D-14-00580.1>
- Torrence C, Compo GP (1998) A practical guide to wavelet analysis. *Bull Am Meteorol Soc* 79:61–78. [https://doi.org/10.1175/1520-0477\(1998\)079<0061:APGTWA>2.0.CO;2](https://doi.org/10.1175/1520-0477(1998)079<0061:APGTWA>2.0.CO;2)
- Torrence C, Webster PJ (1998) The annual cycle of persistence in the El Niño/Southern Oscillation. *Q J R Meteorol Soc* 124:1985–2004
- Trenberth KE, Stepaniak DP (2001) Indices of El Niño evolution. *J Clim* 14:1697–1701. [https://doi.org/10.1175/1520-0442\(2001\)014<1697:LIOENO>2.0.CO;2](https://doi.org/10.1175/1520-0442(2001)014<1697:LIOENO>2.0.CO;2)
- Ueda H, Matsumoto J (2000) A possible triggering process of east-west asymmetric anomalies over the Indian Ocean in relation to 1997/98 El Niño. *J Meteorol Soc Jpn* 78:803–818. [https://doi.org/10.2151/jmsj1965.78.6\\_803](https://doi.org/10.2151/jmsj1965.78.6_803)
- Ummenhofer CC, England MH, McIntosh PC et al (2009) What causes southeast Australia's worst droughts? *Geophys Res Lett* 36:1–5. <https://doi.org/10.1029/2008GL036801>
- Wang B, Chan JCL (2002) How strong ENSO events affect tropical storm activity over the western North Pacific. *J Clim* 15:1643–1658. [https://doi.org/10.1175/1520-0442\(2002\)015<1643:HSEEAT>2.0.CO;2](https://doi.org/10.1175/1520-0442(2002)015<1643:HSEEAT>2.0.CO;2)
- Webster PJ, Holland GJ, Curry JA, Chang HR (2005) Changes in tropical cyclone number, duration, and intensity in a warming environment. *Science* 309(5742):1844–1846. <https://doi.org/10.1126/science.1116448>
- Webster PJ, Moore AM, Loschnigg JP, Leben RR (1999) Coupled ocean-atmosphere dynamics in the Indian Ocean during 1997–98. *Nature* 401:356–360. <https://doi.org/10.1038/43848>
- Wu MC, Chang WL, Leung WM (2004) Impacts of El Niño–Southern Oscillation events on tropical cyclone landfalling activity in the western North Pacific. *J Clim* 17:1419–1428. [https://doi.org/10.1175/1520-0442\(2004\)017<1419:IOENOE>2.0.CO;2](https://doi.org/10.1175/1520-0442(2004)017<1419:IOENOE>2.0.CO;2)
- Xu J, Chan JCL (2001) The role of the Asian–Australian Monsoon system in the onset time of El Niño events. *J Clim* 14:418–433. [https://doi.org/10.1175/1520-0442\(2001\)014<0418:TROTA>2.0.CO;2](https://doi.org/10.1175/1520-0442(2001)014<0418:TROTA>2.0.CO;2)
- Yeh SW, Wang X, Wang C, Dewitte B (2015) On the relationship between the North Pacific climate variability and the central Pacific El Niño. *J Clim* 28:663–677. <https://doi.org/10.1175/JCLI-D-14-00137.1>
- Yuan JP, Cao J (2013) North Indian Ocean tropical cyclone activities influenced by the Indian Ocean Dipole mode. *Sci China Earth Sci* 56:855–865. <https://doi.org/10.1007/s11430-012-4559-0>
- Yuan Y, Li CY (2008) Decadal variability of the IOD–ENSO relationship. *Chin Sci Bull* 53:1745–1752. <https://doi.org/10.1007/s11434-008-0196-6>
- Zhou Q, Wei L, Zhang R (2019) Influence of Indian Ocean Dipole on tropical cyclone activity over western North Pacific in boreal autumn. *J Ocean Univ China* 18:795–802. <https://doi.org/10.1007/s11802-019-3965-8>

**Publisher's Note** Springer Nature remains neutral with regard to jurisdictional claims in published maps and institutional affiliations.

Springer Nature or its licensor (e.g. a society or other partner) holds exclusive rights to this article under a publishing agreement with the author(s) or other rightsholder(s); author self-archiving of the accepted manuscript version of this article is solely governed by the terms of such publishing agreement and applicable law.